XUV collisional absorption of warm dense aluminium

Contact *bkettle01@qub.ac.uk*

B. Kettle, T. Dzelzainis, S. White, L. Li, B. Dromey, M. Zepf, C. L. S. Lewis, D. Riley

Queen's University Belfast
University Rd, Belfast, BT7 1NN

R. Heathcote, C. Spindloe, S. Spurdle

Central Laser Facility
Rutherford Appleton Laboratory, Didcot, OX11 0WX, UK

G. O. Williams, S. Künzel, M. Fajardo

GoLP/Instituto de Plasmas e Fusão Nuclear,
Instituto Superior Técnico 1049-001 Lisboa, Portugal

A. Rigby, G. Gregori

Clarendon Laboratory,
Oxford, OX1 3PU, UK

H. Dacasa, Ph. Zeitoun

Laboratoire d'Optique Appliquée,
91761 Palaiseau Cedex, France

Introduction

The properties of warm dense matter (WDM) are of interest to many scientists, especially those concerned with the structure of giant planets, where WDM conditions (1-100eV and >0.1g/cc) are thought to be common. There are many aspects of WDM that can be addressed experimentally, such as equation of state [1], electrical and thermal conductivity, and microscopic structure [2].

In the experiment described we investigate the collisional absorption (or free-free opacity) of Al in the WDM state for the XUV regime. This regime assumes that the absorption processes are governed solely by the photons interacting with the free or valence electrons of the aluminium, i.e. bound-bound and bound-free transitions play very little or no role. It has been a matter of some controversy [3,4] and is theoretically challenging to model as the mechanism by which energy from an XUV beam is absorbed changes from involving electron-phonon collisions at low temperature to electron-ion collisions at higher temperature when the matter has a plasma nature. We consider only photon energies above the cold Al plasma frequency (15.8eV), yet lower than the L-edge (72.6eV). Any lower and the Al is highly reflective, any higher and the bound L-shell electrons will begin to photo-ionise, and bound-free effects would need to be considered. Without this ionisation collisional absorption will be the dominant mechanism for coupling energy to the target. It is also important to note that calculations show that when raising the temperature of an aluminium sample, for solid density and thermal equilibrium the L-shell electrons should not ionise until above the Fermi temperature ($\approx$11eV) [5]. This means heating the sample up to 11eV (well within the warm dense parameter space) should not cause any L-shell electrons to ionise.

In this experiment we use radiative x-ray heating to raise thin foil aluminium samples to temperatures of approximately 1eV. A high harmonics (HHG) probe of multiple XUV wavelengths is then used to probe the absorption of the sample while it is still at solid density.

Experimental Setup

The experiment was conducted at VULCAN Target Area West and the setup is illustrated in figure 1. The six VULCAN long pulse beams were used in a 200ps Gaussian FWHM configuration, and all were frequency doubled (2ω) to 526.5nm using six KDP II crystals. The beams were split into two sets of three before entering the chamber. Each set of three beams provides up to 110±5J in total energy, and each beam is individually focussed to a $\approx$210µm elliptical flat top spot using hybrid phase plates (resulting in $\approx$2x10^{15}W/cm^2). This configuration replicates a previous experimental configuration for generating hard x-rays from palladium coated CH heater foils. The results have recently been accepted for publication in *Journal of Physics B, July 2015*. The x-ray yield from the palladium-coated heater foils is concentrated around the M-L band (3-3.5keV), and was diagnosed using crystal based spectrometers, deployed on every shot. An x-ray streak camera (XRSC) and x-ray pinhole camera were also deployed to characterise the temporal and spatial properties of the emission. Hydrodynamic simulations based on the palladium emission and a blackbody model were used to simulate the heating of a thin aluminium sample foil placed at 45° in between two heater foils, 2mm apart. The target layout can be seen in figure 2.
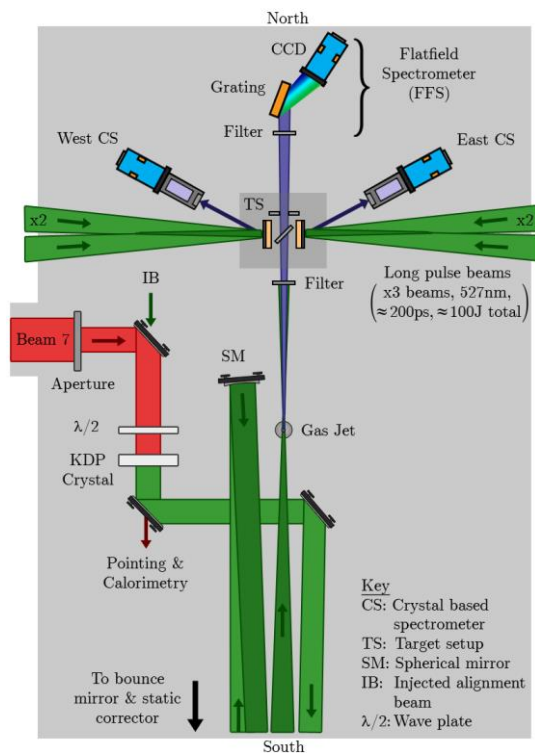

Figure 1. TAW chamber layout. The main target setup (TS) is positioned in the centre of the top half of the chamber. It is irradiated from both sides by the long pulse beams. The HHG probe is generated using beam 7 and travels south to north through the sample target before entering the flatfield spectrometer.
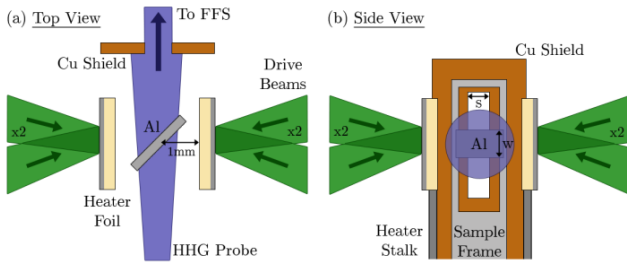
Figure 2. Target setup: (a) Top view looking down at the horizontal plane. Two heater foils surround the Al sample to bathe it in hard x-rays, while still allowing the HHG probe to propagate through. (b) Side view looking along the HHG probe axis. The footprint of the harmonic beam is highlighted by the shaded circle. It passes though the aluminium sample strip supported by the steel frame. The copper shield is also visible in the background.

After the long pulse beams strike the heater foils, M-L band x-ray emission from the palladium bathes the aluminium sample, radiatively heating it to warm dense matter conditions. At some time after heating, the HHG probe passes through the sample target region and onwards to a spectrometer. A copper shield with a 1mm wide slit (s) restricts only XUV radiation from the probe travelling to the detector. It blocks the direct line of sight between the Pd foils and the FFS. A fiducial timing system was used for accurate calibration of the time at which the sample was probed (within 10ps). Figure 2 (b) depicts the target setup looking along the HHG axis. The aluminium sample is stretched across a steel frame. It is a narrow 500μm (w) wide strip. The shaded circle represents the HHG probe propagating towards the spectrometer (into the page). While a portion of the HHG beam will pass through the sample, part of it will also travel unhindered towards the detector. A comparison of the clear rays to the attenuated rays provides the XUV transmission of the heated sample.

The short pulse beam 7 is used to generate the HHG probe. It enters the chamber from the west and is immediately apertured down to 70mm diameter. The beam then passes through a half wave plate and its polarisation is rotated by 90°. After this the beam is frequency doubled using a KDP crystal, each pulse containing between 200-500mJ. The beam is directed onto a 5m focal length spherical mirror at near normal incidence, before being focused down through an argon gas jet to create the harmonics. This probe beam propagates along the south-north axis of the chamber through the sample target and onto a spectrometer for collection. After the gas jet, a thin aluminium filter before the sample stops the drive laser from propagating further, while passing the XUV harmonics albeit at a reduced intensity. The primary diagnostic used to assess the harmonic probe is a flatfield spectrometer (FFS). The grating was tilted at 4° to the incoming beam and the CCD plane was at 74° to the beam.

Results

Over the course of the experiment run over 50 full data shots were taken. However, due to fluctuations in the harmonic probe, and the random jitter of the beam synchronisation (±150ps), a fraction of these data shots were considered useful. Another problem arose in the spatial uniformity of the harmonics probe. Large variations in the yield can be seen across the spatial axis. On top of this, the profile fluctuated between each shot, under the same gas jet and laser conditions. The relatively long pulse (1ps) and high energy of the drive laser pulse used may be ionising the gas medium and causing regions of decreased generation, or even refraction of the beam. Another explanation may stem from the shape of the drive beam focal spot. Unfortunately the profile of the beam away from tight focus was found to be very astigmatic and disrupted.

Cold Transmission

Without any of the long pulse beams (or heating x-rays), the transmission of room temperature ("cold") aluminium can be measured. Figure 3 (a) shows an example cold shot on a 218nm aluminium sample. The spectral dispersion in the image goes from left to right, with increasing wavelength (or decreasing energy), and the vertical axis is the spatial axis of the detector. The visible HHG orders are 13th, 11th, and 9th from left to right.
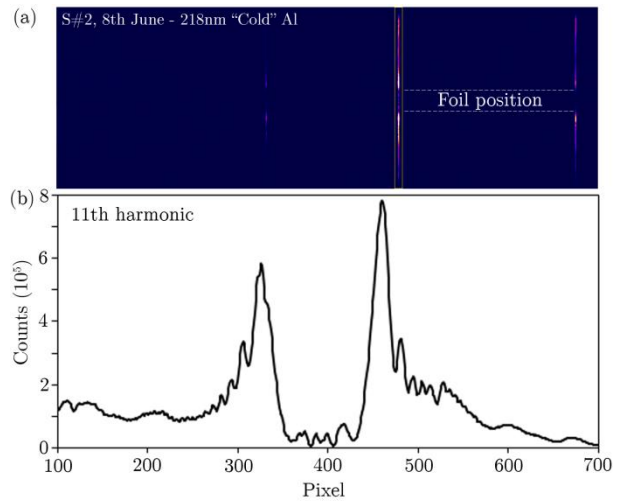

Figure 3. A "cold" data shot (#2, 8th June) for a 218nm Al sample. (a) Raw flatfield spectrometer data with the 9th, 11th and 13th order harmonics visible. The spatial position of the foil has been highlighted. (b) Lineout of the 11th harmonic across the spatial direction.

The position of the sample foil in the spatial axis is highlighted and a lineout across the spatial axis of the 11th harmonic can be seen in (b). The presence of the foil can clearly be seen in the centre of the profile where there is a large drop in signal. The small oscillating pattern seen overlaid in the general shape of the profile is understood to be diffraction from the edges of the foil. This must be accounted for in the transmission analysis.

WDM Transmission

An example of a full data shot can be seen in figure 4. The aluminium sample foil in place was 218nm thick, and all the long pulse beams were fired at full power to create the heating x-rays. The probe time was found from the fiducial to be 200ps after onset of the x-ray heating.
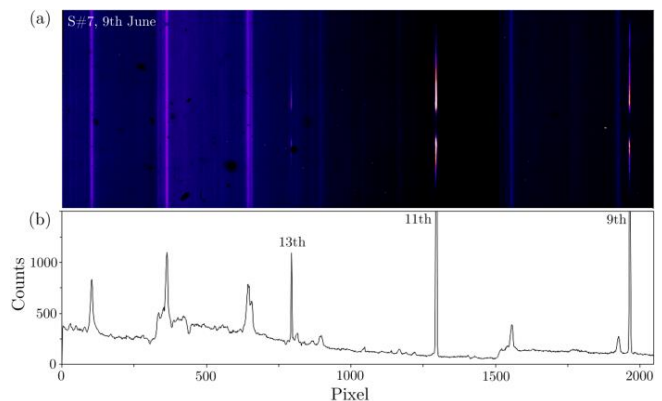

Figure 4. A full data shot with all the long pulse beams and the harmonics probe. (a) The raw flatfield data and (b) a lineout averaged along the spatial direction. Additional spectral lines and background can clearly be seen alongside the expected harmonic signal.

The raw image from the FFS can be seen in (a), and an averaged lineout across the spectral axis can be seen in (b). The first clear observation is the presence of large amounts of new

background emission alongside the usual harmonic orders seen previously. This background profile is of the same shape and yield for each shot that the heater foils were used. It is understood to be higher order reflections of soft x-ray carbon lines from the CH backing of the heater foils. There is a copper shield present in the target setup to select only radiation from the aluminium sample region. However, the capture time of the CCDs used is of the order of 100s of milliseconds, which is more than enough time for the heater foils to expand and travel towards the target centre. This plasma plume reaches the aluminium target position long after the harmonics beam, however the plume is still hot enough to have significant x-ray emission which will be overlaid on top of our probe signal on the detector. Fortunately as the shape of the background is consistent between each shot, and in fact relatively flat in the section of the detector the harmonic lines are present, it can easily be subtracted from the signal.

Target Conditions

HYADES (a 1-D radiation hydrodynamics simulation package) [7] simulations were carried out to estimate the sample temperature and density as a function of time. We assume the energy deposition is transferred to the sample via the three valence electrons, and that it follows a spectral yield based on the data from the crystal spectrometers and a temporal profile similar to that of the measured x-ray pulse. Although only true to the variations mentioned above, as HYADES is a 1-D simulation code, the energy deposition was taken as spatially uniform. Figure 5 depicts the density and temperature of one of the data shots used. Over 65% of the target remains at solid density with a temperature of 0.95eV. These are ample WDM conditions and perfect for comparison to the conflicting models of [3] and [4].
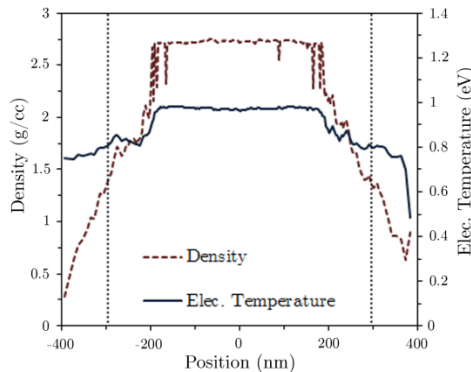
Figure 5. The density (red dashed) and electron temperature (blue solid) for shot #6 on 9/6/2015, a 418nm Al foil (at 45°) probed 108ps after heating. The original foil edge positions can be seen by the vertical dashed lines.

Diffraction effects

It is clear the interpretation of the results presented is not as straight forward as expected. We have already discussed the subtraction of the unwanted background signal, but another major issue is the diffraction effects present in the spatial profile of the harmonics. Understanding this phenomenon is crucial to calculating its influence and making an accurate transmission measurement. Based on the Huygens-Fresnel principle a simulation code for the experiment setup has been written.

Figure 6 shows the estimated input beam profile (red dashed line) and the simulated diffraction profile (blue dotted line) compared to the real data (black solid line) of shot #2 on 11th June 2015. The sample is a cold 838nm Al foil.
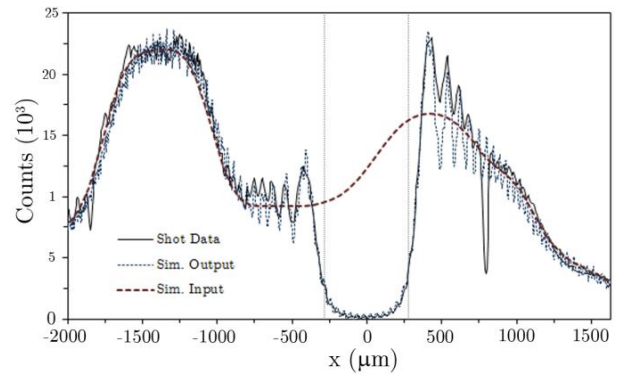
Figure 6. Simulation input (red dash) and output (blue dots) compared to the real data (black solid) of shot #2, 11/6/2015. The sample is a cold 838nm Al foil (centred at x=0). The position of the foil edges are highlighted with the vertical dotted lines.
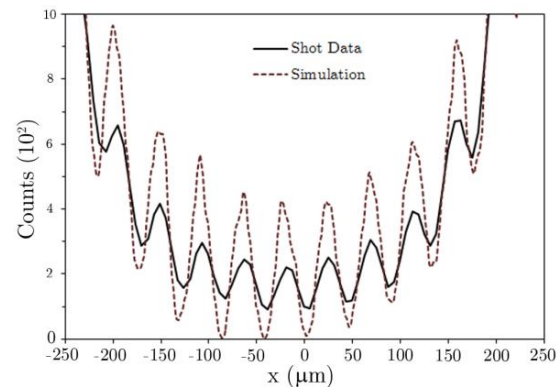
Figure 7. A close-up view of the foil shadow region of figure 6. The position of the peak structures of both the real data and simulation match well.

It seems very possible to reproduce the effect of placing a foil in the path of the harmonics profile, and to estimate the amount of signal that would spread into the shadow region. With this information a comparison of diffracted signal to the measured signal can be used to give a transmission measurement, and hence a value for the absorption coefficient. Figure 7 depicts a close-up view of the foil shadow region of figure 6. The interference pattern positions of the real data compare extremely well to the simulation output. The peaks occur at the same positions in both cases. The magnitude of the peaks and troughs of the data however seem smaller in comparison to the simulation. It is believed that this is due to resolution of the detector and the source size of the harmonics, and that the intensity of the signal is being smeared on a small scale across the profile. The data shown is for a cold harmonics shot on an Al sample foil of thickness of 838nm. For this sample thickness the estimated transmission is less than 0.08%; there should be essentially no detectable transmission taken to penetrate the sample. Integrating the total signal underneath the simulated profile between the two foil edges is found to be equivalent to the integrated shot data within the same limits (to within 0.05%, well within our error margins). The signal detected in the foil shadow on the shot is nearly completely due to diffracted light from the foil edges. This matches the transmission prediction and gives strong evidence for the accuracy of the diffraction simulations. The simulation code is currently being modified to include the effects of phase change as the harmonic beam passes through the aluminium foil.

Conclusions

Analysis of the results is on-going but there is strong evidence that the experimental technique described can help distinguish

between the competing models for the collisional absorption of aluminium in both cold and WDM conditions.

A large uncertainty in the results follows from the uncertain profile of the direct harmonic (before transmission) and having to estimate the signal in this region. Modifying the experimental geometry to allow a simultaneous measurement of both direct and transmitted signal should prove to be a sizeable improvement in the accuracy of the results. One possible method for this would involve placing the sample after the diffraction grating and relying on a measurement of a high order reflection for the direct signal. The symmetric output of a transmission grating could also be utilised. Another unforeseen complication in the processing of the data is the presence of the diffraction and interference patterns from the sample foil edges. The use of a wider foil would reduce the interference from the two edges.

References

1. P. Renaudin, C. Blancard, J. Clérouin, G. Faussurier, P. Noiret, and V. Recoules, *Phys Rev. Lett*. **91**, 7 075002-1 (2003).

2. S. White, G. Nersisyan, B. Kettle, T.W.J. Dzelzainis, K. McKeever, C.L.S. Lewis, A. Otten, K. Siegenthaler, D. Kraus, M. Roth, T. White, G. Gregori, D.O. Gericke, R. Baggott, D.A. Chapman, K. Wünsch, J. Vorberger, D. Riley, *High Energy Density Physics* **9**, 573-577 (2013).

3. S. Vinko, G. Gregori, M. P. Desjarlais, B. Nagler, T. J. Whitcher, R. W. Lee, P. Audebert, J. S. Wark, *High Energy Density Physics* **5**, 124-131 (2009).

4. C. Iglesias, *High Energy Density Physics* **6**, 311-317 (2010).

5. D. Kim and I. Kim, *Phys. Rev. E* **68**, 056410 (2003).

6. D. W. Phillion and C. J. Hailey, *Phys. Rev. A* **34**, 4886 (1986).

7. J. T. Larsen and S. M. Lane, *J. Quant. Spectrosc. Radiat. Transfer* **51**, 179–186 (1994).